1996

Determination of Transport and Electrochemical Kinetic Parameters of Bare and Copper-Coated $LaNi_{4.27}Sn_{0.24}$ Electrodes in Alkaline Solution

G. Zheng
University of South Carolina - Columbia

Branko N. Popov
University of South Carolina - Columbia, popov@engr.sc.edu

Ralph E. White
University of South Carolina - Columbia, white@cec.sc.edu

Publication Info

Journal of the Electrochemical Society, 1996, pages 834-839.

Publisher's link: http://dx.doi.org/10.1149/1.1836545
DOI: 10.1149/1.1836545

Determination of Transport and Electrochemical Kinetic Parameters of Bare and Copper-Coated $LaNi_{4.27}Sn_{0.24}$ Electrodes in Alkaline Solution

G. Zheng,* B. N. Popov, and R. E. White**

Department of Chemical Engineering, University of South Carolina, Columbia, South Carolina 29208, USA

ABSTRACT

Electrochemical properties of bare and copper-coated $LaNi_{4.27}Sn_{0.24}$ electrodes were investigated in alkaline solution. The exchange current density, polarization resistance, and equilibrium potential were determined as functions of the state of charge in the electrodes. The symmetry factors for bare and copper-coated electrodes were estimated to be 0.53 and 0.52, respectively. By using a constant current discharge technique, the hydrogen diffusion coefficient in bare and coated $LaNi_{4.27}Sn_{0.24}$ was estimated to be 6.75×10^{-11} cm^2/s.

Introduction

The development of metal hydride electrodes has been reviewed by Bittner and Badcock[1] and Willems.[2] The performance of a metal hydride electrode is determined by both the kinetics of the processes occurring at the metal-electrolyte interface and the rate of hydrogen diffusion within the bulk of the alloy.[3-7] Yayama *et al.*[8] measured the equilibrium potential and exchange current density as functions of hydrogen content in $TiMn_{1.5}H_x$ ($x < 0.31$). An analysis of the kinetics in metal hydride electrodes carried out by Van Rijswick[9] shows that for small-size particles charge-transfer is the rate-limiting step and for large particles hydrogen transport in the solid is the rate-limiting step. For $LaNi_4Cu$, Van Rijswick[9] found an exchange current density of 0.5 mA/cm^2, which is on the order of exchange current density for highly catalytic metals such as Pt and Pd, and he estimated the hydrogen diffusion coefficient to be 7×10^{-10} cm^2/s. Sakai *et al.*[10] investigated the effects of microcapsulation of $LaNi_{4.7}Al_{0.3}$ with a porous, thin film of copper. They found that the cycle life and charge-discharge characteristics of the electrode were improved by the copper, especially at high rates and low temperatures due to the role of copper as an oxygen barrier for protecting the alloy surface from oxygen and as a microcurrent collector for facilitating a charge-transfer reaction on the alloy surface. Zuchner *et al.*[11] used the current-pulse method to measure the hydrogen diffusion coefficient in the α-phase of M-H in $LaNi_5$. The temperature dependence of the diffusion coefficients was found that is best described by the Arrhenius expression.

Mendelsohn *et al.*[12] used Sn as a partial substitute for Ni in $LaNi_5$. They found that this alloy has an absorption capacity corresponding to $LaNi_{4.6}Sn_{0.4}H_{5.80}$. According to Chandra *et al.*,[13,14] tin enhances the durability of an alloy. Electrochemical evaluation of Sn-modified $LaNi_5$ was carried out by Ratnakumar *et al.*[15] They found that substituting a small amount of Sn for Ni provides a large improvement in the capacity and cycle lifetime of the electrode and improves the kinetics of hydrogen absorption-desorption processes. Ratnakumar *et al.*[15] also made an attempt to correct the Tafel curves for the mass-transfer interference for this alloy. However, they used the same limiting current for the cathodic and the anodic portion of the curves, which are different. The anodic current is limited by the hydrogen diffusion from the bulk of the alloy (solid phase) toward the interface, while the cathodic current is controlled by the H_2O diffusion from the bulk of the electrolyte toward the electrode/electrolyte interface.

The previous work cited above reveals that the transport of hydrogen in the bulk of the alloy, the electrochemical kinetic properties of metal hydride electrodes, and the equilibrium potential are important parameters which characterize the performance of metal hydride electrode. The objective of this research was to determine the exchange current density and the equilibrium potential of bare and copper-coated $LaNi_{4.27}Sn_{0.24}$ electrodes as functions of the state of charge (hydrogen content of the electrode).

Theory

The main electrode reactions that occur at a metal hydride electrode are

$$M + H_2O + e^- \rightleftarrows MH_{ads} + OH^- \quad [1]$$

$$MH_{ads} \rightleftarrows MH_{abs} \quad [2]$$

and

$$MH_{abs} \rightleftarrows MH_{hyd} \quad [3]$$

where H_{ads}, H_{abs}, and H_{hyd} represent a hydrogen atom adsorbed on the surface, absorbed on the surface, and in the form of hydride, respectively. The microkinetic current density (i'), *i.e.*, the current per unit of electroactive surface area of the electrode for reaction 1, can be written as[16]

$$i' = i_o' \left[\frac{C_{H_2O(p)}}{C_{H_2O(b)}} \exp\left(\frac{-\beta F}{RT}\eta\right) + \frac{C_{OH^-(p)}}{C_{OH^-(b)}} \exp\left(\frac{(1-\beta)F}{RT}\eta\right) \right] \quad [4]$$

where C_i are the concentration of species i, β is the symmetry factor, F is the Faraday constant, R is the gas constant, T is the temperature, and η is the overpotential, which is a function of position in the porous electrode. The subscripts "p" and "b" represent the "pore" of the electrode and the "bulk" of the electrolyte, respectively.

According to Austin,[16,17] assuming that (*i*) the mass-transfer factors of H_2O and OH^- are the same so that $C_{H_2O(p)} + C_{OH^-(p)} = C_{H_2O(b)} + C_{OH^-(b)}$ and (*ii*) the potential drop through the pore electrolyte is sufficiently small so that the overpotential η is constant, one may obtain the following expression for current density

$$i = i_o \left[\frac{C_{H_2O(i)}}{C_{H_2O(b)}} \exp\left(\frac{-\beta F}{RT}\eta\right) + \frac{C_{OH^-(i)}}{C_{OH^-(b)}} \exp\left(\frac{(1-\beta)F}{RT}\eta\right) \right] \frac{\tanh\left(\sqrt{K}\right)}{\sqrt{K}} \quad [5]$$

and

$$K = \frac{i_o LM}{A_s F D_{H_2O}} \left\{ \frac{\exp\left[-\frac{\beta F\eta}{RT}\right]}{C_{H_2O(b)}} + \frac{\exp\left[-\frac{(1-\beta)F\eta}{RT}\right]}{C_{OH^-(b)}} \right\} \quad [6]$$

* Electrochemical Society Student Member.
** Electrochemical Society Active Member.

where i is the mass current density, *i.e.*, the current per unit of mass of the electrode, L is the half thickness of the electrode, M is the total mass of the electrode, A_s is the cross-sectional area of the electrode, D_{H_2O} is the effective diffusion coefficient of water, and the subscript "i" refers to the interface between the electrode and electrolyte.

If i_oL and η are low, then $\sqrt{K}$ is small so that $\tanh(\sqrt{K})/\sqrt{K} \approx 1$ and if the concentration ratios in Eq. 5 are about one, then Eq. 5 reduces to

$$i = i_o\left[-\exp\left(\frac{-\beta F}{RT}\eta\right) + \exp\left(\frac{(1-\beta)F}{RT}\eta\right)\right] \quad [7]$$

which is the conventional equation for a planar electrode; however, it may be applied only for low overpotentials. Further, Eq. 7 may be linearized as

$$i = i_o\frac{F\eta}{RT} \quad [8]$$

and an equation for polarization resistance (R_p) may be written as

$$R_p = \frac{RT}{Fi_o} \quad [9]$$

Comparison of Eq. 8 and 9 shows that R_p can be determined from a linear polarization curve; once R_p is known Eq. 9 can be used to determine i_o. The symmetry factor (β) cannot be determined from conventional Tafel plots since the Tafel equation does not apply for porous electrodes.[16,17] In order to determine the symmetry factor, β, Eq. 7 may be rewritten as

$$\frac{i}{\exp(F\eta/RT)-1} = i_o\exp(-\beta F\eta/RT) \quad [10]$$

Taking logarithm of Eq. 10, one obtains[18,19]

$$\eta = \frac{2.3RT}{\beta F}\log i_o - \frac{2.3RT}{\beta F}\log\left[\frac{i}{\exp(F\eta/RT)-1}\right] \quad [11]$$

Thus, from the slope of the plot of η *vs.* $\log[i/\exp(F\eta/RT) - 1]$, the symmetry factor can be determined. Equation 11 is only valid in the low overpotential region.

Experimental

Preparation of metal hydride electrodes.—The alloy $LaNi_{4.27}Sn_{0.24}$ was first crushed and ground mechanically. The resulting powder was passed through a 230 mesh sieve, which gave a particle size of less than 63 μm. These particles were then coated with a thin film of copper by electroless copper deposition. The plating process was carried out in steps. The electroless copper deposition carried out in this study was similar to Sakai *et al.*'s[10] method. The alloy surface was activated by immersing the powder in an aqueous HCl solution of $SnCl_2$ and then in an aqueous HCl solution of $PdCl_2$. The activated powder was then immersed in an electroless plating solution containing 30 g/liter $CuSO_4 \cdot 5H_2O$, 100 g/liter sodium potassium tartarate, 50 g/liter NaOH, 32 g/liter Na_2CO_3, and 29 ml/liter HCHO. The copper to alloy ratio was 1/4 by weight, which yielded a thickness of the metallic copper layer less than 1 μm. The electroless plating process was terminated when the deep blue color arising from the copper complex vanished.

Next, pellet electrodes were prepared by mixing the alloy with 2.5 weight percent (w/o) polytetrafluoroethylene (PTFE) followed by pressing the material in a cylindrical press. A 5/16 in. diameter pellet was formed at approximately 300°C using a pressure of 5 ton/cm^2. The mass and the thickness of the pellet were 160 mg and 0.75 mm, respectively. The pellet was then inserted between two pieces of Plexiglas with small holes on each side. The electrode was immersed in the test cell and filled with a 6 *M* KOH electrolyte solution. A good electrical connection to the pellet was achieved through the following procedure: (*i*) a piece of platinum wire was passed several times through a platinum mesh and (*ii*) the platinum mesh and the wire were then pressed together to obtain good electrical contact. A piece of Pt gauze was placed on each side of the electrode and served as counterelectrode. Prior to the experiments the alloy electrode was activated by cycling the electrode ten times.

Charge-discharge characteristics and cyclic voltammograms of this electrode were obtained at 25°C using the Model 342C SoftCorr System with EG&G Princeton Applied Research potentiostat/galvanostat Model 273A. The experiments were carried out using a Hg/HgO reference electrode. The exchange current density and equilibrium potential were determined as functions of hydrogen content in the electrode. Faraday's law was used to determine the hydrogen content of the coated alloy.

Charging and discharging procedure.—The experimental procedure was performed as follows: the electrode was charged under a constant current mode until the hydrogen content reached its saturated value. The equilibrium potential was measured against the Hg/HgO reference electrode. Next, linear polarization experiments were carried out. The measurements were performed only after the open-circuit potential was stabilized (*i.e.*, the change of the potential was less than 1 mV for a period of 1 h). The electrode was discharged for a certain period of time, and the same measurements as above were conducted. This procedure was repeated until the electrode was discharged to the potential of −0.6 V *vs.* Hg/HgO reference electrode.

Results and Discussion

Discharge characteristics.—Typical discharge curves for bare and copper-coated alloys in 6 *M* KOH as a function of state of charge are shown in Fig. 1. Assuming that 5.51 hydrogen atoms are adsorbed by one formula of the alloy, the theoretical capacity was calculated to be 353 mAh/g. The experimental capacity of bare and copper-coated $LaNi_{4.27}Sn_{0.24}$ alloy are 270 and 275 mAh/g, and are about 76 and 78% of the theoretical capacity, respectively.

Initially, the discharge process is charge-transfer control as indicated by the potential plateaux shown in Fig. 1. After a certain period of time, a drastic potential change occurs due to the depletion of hydrogen atoms from the electrode surface. Note that copper-coated electrode has a higher potential than the potential observed for the bare electrode. These phenomena can be explained by taking into account that the polarization resistance R_p of the copper-coated alloy is lower compared with the corresponding resistance of the bare alloy for the same state of dis-

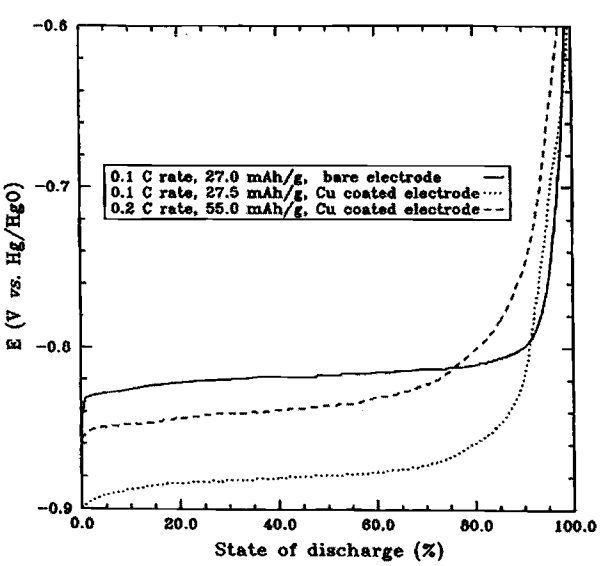

Fig. 1. Typical discharge curves obtained for different discharge rates for a bare and a copper-coated electrode.

charge. According to Eq. 8 and 9, the potential drop during the discharge is proportional to the polarization resistance, R_p. Since copper facilitates the charge-transfer reaction on the alloy surface by decreasing the charge-transfer resistance, the potential drop for the copper-plated alloy is smaller than the potential drop for the bare alloy. However, at the end of discharge, the state of charge of the copper-plated electrode at 0.2 C rate is lower than the state of charge of the bare electrode (0.1 C rate) due to the diffusion limiting effect of hydrogen in the alloy at higher discharge rates.

Determination of the diffusion coefficient of hydrogen through the electrode.—Assuming that the hydride alloy particles are in spherical form, the diffusion equation is

$$\frac{\partial(rc)}{\partial t} = \overline{D}\frac{\partial^2(rc)}{\partial r^2} \qquad [12]$$

where c is the concentration of hydrogen in the alloy, t is time, $\overline{D}$ is an average (or integral) diffusion coefficient of hydrogen over a defined concentration range, and r is a distance from the center of the sphere. Since the discharge process was carried out under a constant current condition, it is reasonable to assume that a constant flux of the species at the surface applies and uniform initial concentration of hydrogen in the bulk of the alloy. Thus, the value of $\overline{D}/a^2$ may be evaluated for large transitions times, τ[20]

$$\frac{\overline{D}}{a^2} = \frac{1}{15\left(\frac{Q_o}{i} - \tau\right)} \qquad [13]$$

where Q_o is the initial specific capacity (C/g), i is the current density (A/g), and τ is transient time (s), (*i.e.*, the time required for the hydrogen surface concentration to become zero.) The ratio Q_o/i corresponds to the discharge time necessary to discharge completely the electrode under hypothetical conditions when the process proceeds without interference of diffusion. Rearranging Eq. 13, one obtains

$$Q_1 = Q_o - \tau i = \frac{i}{15}\frac{a^2}{\overline{D}} \qquad [14]$$

where Q_1 is the charge left in the electrode when the hydrogen surface concentration is zero. According to Eq. 14, the charge (*i.e.*, hydrogen content) left in the electrode after discharge is proportional to the discharge current, i (A/g), and to the square of the particle size, and is inversely proportional to the hydrogen diffusion coefficient.

The galvanostatic discharge curves presented in Fig. 1 may be used to estimate the hydrogen diffusion coefficient by determining the transition time τ. The galvanostatic discharge curves presented in Fig. 1 were obtained at a constant current per unit mass of 27.0 mAh/g for the bare electrode and at 27.5 and 55.0 mAh/g for the copper coated electrode. The experiments were terminated at a potential of −0.6 V *vs.* Hg/HgO reference electrode. The estimated transition times obtained at a constant current per unit mass of 27.0 mAh/g for the bare electrode and 27.5 mAh/g for the copper-coated electrode were 9.40 and 9.38 h, respectively. The initial charge of the electrode, Q_o was 972 C/g (270 mAh/g) for the bare electrode and 990 C/g for the copper-coated electrode. Thus, the calculated value of $\overline{D}/a^2$ using Eq. 13 is 3.1×10^{-5} and 3.0×10^{-5} s^{-1}, respectively, which is close to our previous estimated value of $\overline{D}/s^2$ through a $LaNi_{4.25}Al_{0.75}$ electrode of 1.42×10^{-5} s^{-1}.[20] Assuming that the average particle radius $a = 15$ μm, the effective diffusion coefficient through $LaNi_{4.27}Sn_{0.24}$ was calculated to be 6.75×10^{-11} cm^2/s. The charge remaining in the electrode after discharge for τ s was estimated to be 58 C/g for the bare electrode and 61 C/g for the copper-plated electrode.

Cyclic voltammetry.—To illustrate the processes that occur during charge and discharge of the electrode, a cyclic voltammetry study was carried out at different sweep rates in the range from −0.70 to −1.20 V *vs.* Hg/HgO reference electrode. As shown in Fig. 2 and 3, broad discharge current peaks occurred at approximately −1.02 V *vs.* Hg/HgO reference electrode for sweep rates of 0.5 mV/s or less, which corresponds to hydrogen desorption from the metal hydride. In Fig. 2 the hydrogen desorption peak was not observed at high sweep rates (v = 100 and 10 mV/s) indicating that the hydride formation during the cathodic cycle was negligible due to the very short charge times (10 and 100 s, respectively). The hydrogen desorption starts to occur at a sweep rate of 1 mV/s and the desorption peaks become large when smaller sweep rates (v = 0.5, 0.2, 0.1, and 0.07 mV/s) are used. These phenomena can be explained by taking into account that: (*i*) at low sweep rates the hydrogen concentration on the surface increases due to longer polarization in cathodic direction; (*ii*) the hydrogen concentration approaches a value which favors metal hydride formation. Since the curves presented in Fig. 2 and 3 were obtained in sequence, one after another, from high to low sweep rates, one can assume that hydrogen accumulates in the alloy. At high sweep rates (100 and 10 mV/s) the total hydrogen absorbed was 0.30 and 2.79 mAh/g, respectively, and

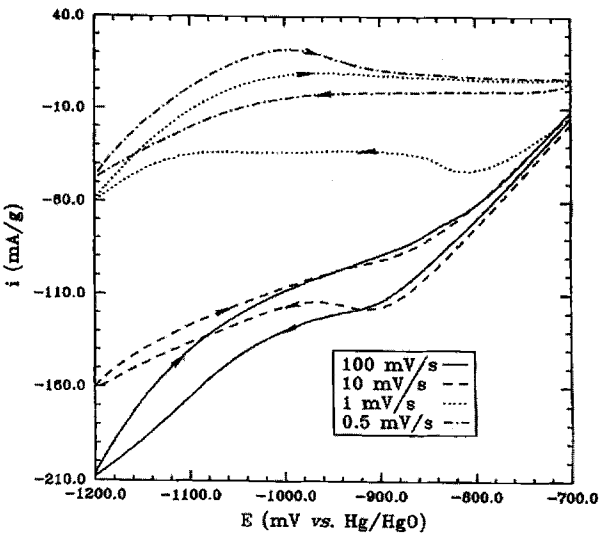

Fig. 2. Cyclic voltammetry curves obtained at different scan rates on the copper-coated electrode.

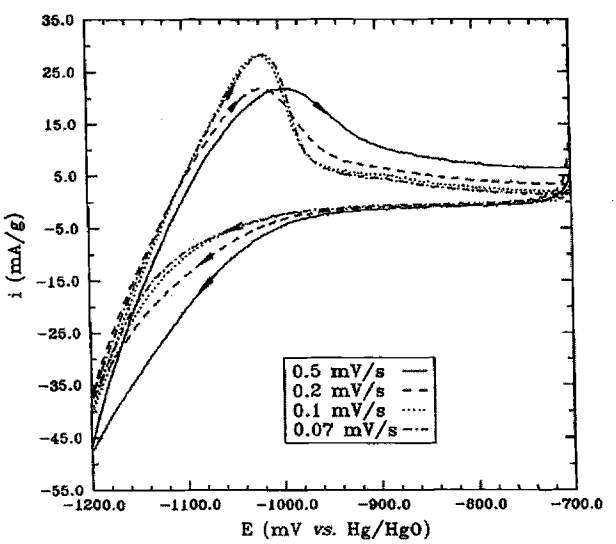

Fig. 3. Cyclic voltammetry curves obtained at different scan rates on the copper-coated electrode.

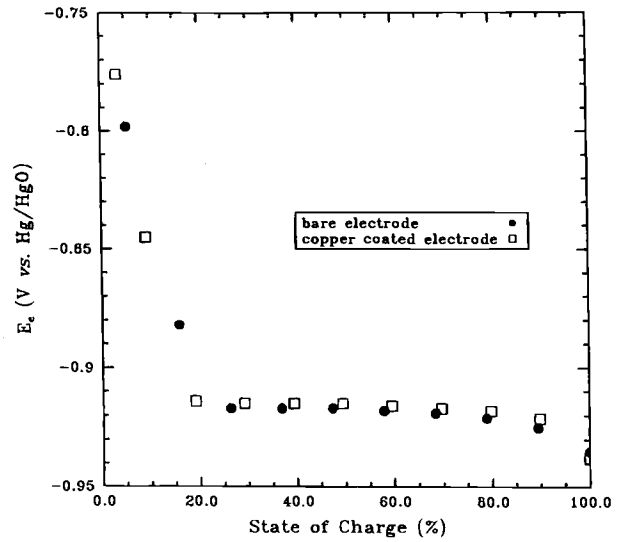

Fig. 4. Equilibrium potential of the bare and copper-coated electrodes as a function of state of charge.

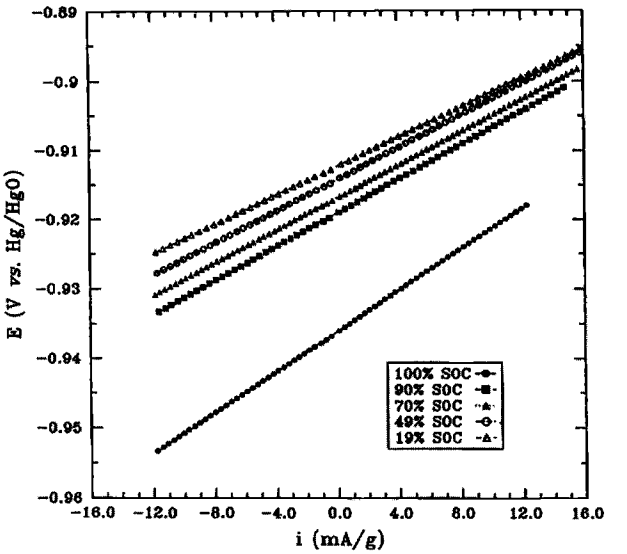

Fig. 6. Typical linear polarization curves of the copper-coated electrode at different states of charge.

equals 3.09 mAh/g. The estimated total charge of 3.09 mAh/g is less than 0.9% of the theoretical state of charge. The charges were estimated by integrating the areas under the cathodic curves. At sweep rate of 1 mV/s, the cathodic charge was 5.96 mAh/g. As shown in Fig. 2 a desorption peak occurs with a charge of 0.66 mAh/g. Thus, the total charge from the first three sweeps before the desorption peak occurred was about 2.6% of state of charge. At a sweep rate of 0.5 mV/s, the cathodic charge was 3.76 mAh/g, which is less than the previous sweep (5.96 mAh/g). However, the desorption charge was 2.58 mAh/g, which is much larger than the previous one (0.66 mAh/g) and is due to hydrogen accumulation on the electrode from the previous sweeps. Consequently, one cannot expect the desorption peak to occur unless the electrode is more than 2% charged. For the lowest sweep rate of 0.07 mV/s, the cathodic charge was 17.00 mAh/g and desorption charge was 13.52 mAh/g, which is 80% of the cathodic charge.

Dependence of equilibrium potential upon state of charge.—The equilibrium potential (E_e) as a function of state of charge for the bare and copper-coated alloys are presented in Fig. 4. The state of charge is defined as a ratio between the amount of charge in the electrode and experimentally measured maximum possible charge in the electrode. As shown in these figures, two phases exist. When the state of charge of the electrodes is less than about 20%, the equilibrium potential of the electrode changes rapidly with hydrogen content. This region, the so-called α-phase, is a solid solution phase. When the hydrogen content continues to increase, then the equilibrium potential more or less keeps constant. This plateau region indicates the formation of β-phase (hydride phase) and at this region two phases (α and β) coexist. Finally, when the hydrogen content increases to about 90% of the state of charge, another steep slope occurs, which indicates the β-phase.

Polarization studies.—Linear polarization studies have been carried out on both bare and copper-coated electrodes at different states of charge. The typical linear polarization curves are presented in Fig. 5 and 6 for bare and copper-coated electrodes, respectively. The exchange current density was estimated using Eq. 8 at different states of charge for both electrodes. The calculated exchange current density were plotted against the state of charge in Fig. 7. Comparing the exchange current density

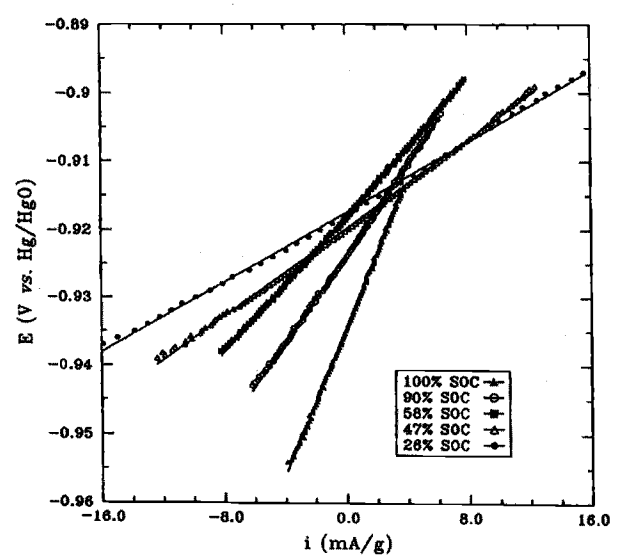

Fig. 5. Typical linear polarization curves of the bare electrode at different states of charge.

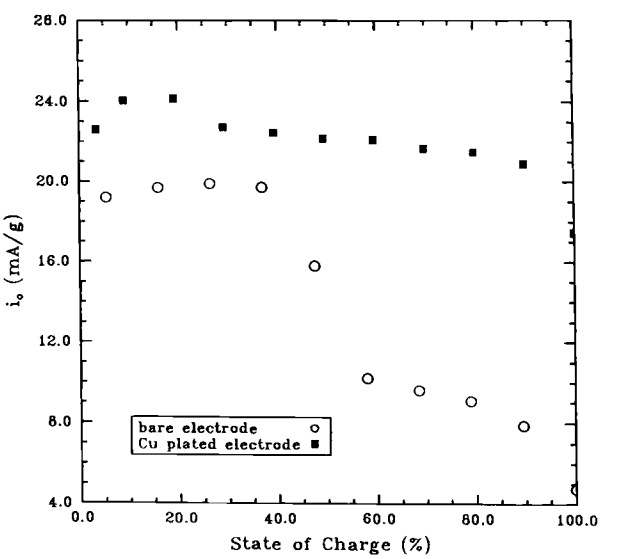

Fig. 7. Exchange current density of the bare and copper electrodes as a function of the state of charge.

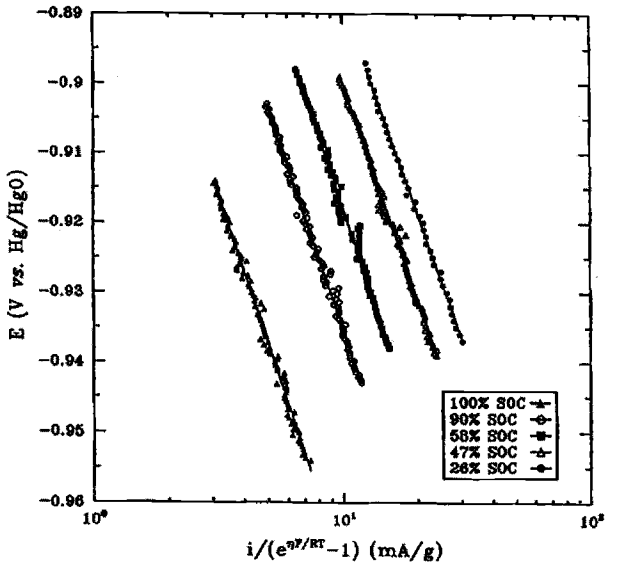

Fig. 8. Dependence of E upon $i/\exp(\eta F/TR) - 1$) for the bare electrode at different states of charge.

values presented in Fig. 7 it can be seen that the copper coating increases the exchange current density which is favorable for the battery operation; this is particularly true for high hydrogen content. For a fully charged electrode (100% state of charge) the exchange current increases from 4.75 mA/g for the bare electrode to 17.5 mA/g for the copper-coated electrode. Similarly, the calculated polarization resistances using Eq. 9 as a function of state of charge indicated that the polarization resistance of the copper-plated alloy is lower when compared with the corresponding resistance estimated for the bare alloy for the same state of charge and is consistent with the conclusion made from discharge curves. The copper coating acts as a microcurrent collector and facilitates the charge-transfer reaction on the alloy surface.

In order to determine the symmetry factor by using Eq. 11, the linear polarization curves in Fig. 5 and 6 were replotted accordingly and are presented in Fig. 8 and 9. As shown in Fig. 8 and 9 a linear relationship exists between η and $\log [i/\exp(F\eta/RT) - 1]$. The symmetry factor was evaluated to be 0.53 for the bare electrode and 0.52 for the copper-coated electrode and does not depend upon hydrogen content in the electrodes.

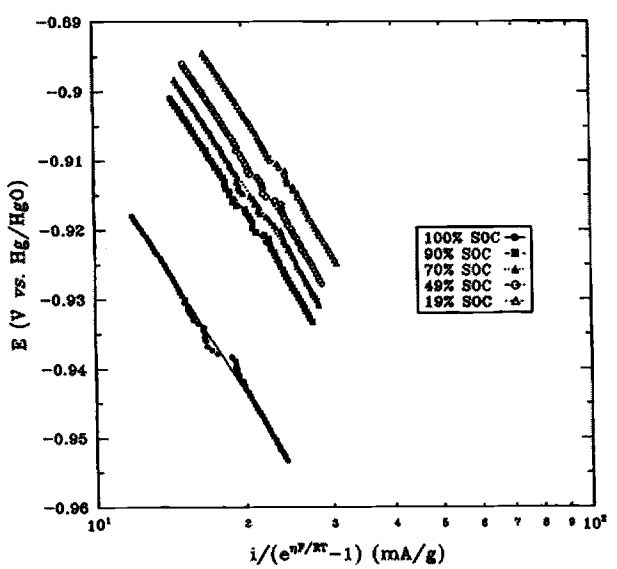

Fig. 9. Dependence of E upon $i/\exp(\eta F/TR) - 1$) for the copper-plated electrode at different states of charge.

Conclusion

Electrochemical properties of bare and copper-plated $LaNi_{4.27}Sn_{0.24}$ electrodes were investigated in alkaline solution. According to our polarization studies, the polarization resistance of a copper-coated alloy was lower when compared with the corresponding resistance estimated for the bare alloy for the same state of charge. The copper coating acts as a microcurrent collector and facilitates the charge-transfer on the alloy surface. Consequently, the copper coating increases the exchange current density and therefore enhances the performance of the electrode. The symmetry factor for bare and copper-plated electrodes was estimated to be approximately 0.53 and 0.52, respectively. The constant current discharge technique was used to determine the hydrogen diffusion coefficient in $LaNi_{4.27}Sn_{0.24}$. The estimated value for the hydrogen diffusion coefficient was 6.75×10^{-11} cm^2/s.

Acknowledgment

Financial support by the Exploratory Technology Research (ETR) Program, which is supported by the Office of Transportation Technologies (OTT) of the U.S. Department of Energy (DOE), Subcontract No. 4614610 is acknowledged gratefully.

Manuscript submitted June 5, 1995; revised manuscript received Dec. 27, 1995.

The University of South Carolina assisted in meeting the publication costs of this article.

LIST OF SYMBOLS

a	sphere radius, cm
A_s	the exposed surface area of the electrode, cm^2
c	hydrogen concentration in the alloy, mol cm^{-3}
C_{H_2O}	concentration of H_2O, mol cm^{-3}
C_{OH^-}	concentration of OH^-, mol cm^{-3}
D	the effective diffusion coefficient, cm^2 s^{-1}
$\bar{D}$	integral diffusion coefficient of hydrogen, cm^2 s^{-1}
E	applied potential, V
E_e	equilibrium potential, V
F	Faraday's constant, 96,487 C eq^{-1}
i	current per unit of mass, A g^{-1}
i_o	exchange current per unit of mass, A g^{-1}
i'	microkinetic current, A cm^{-2}
i'_o	microkinetic exchange current density, A cm^{-2}
K	a constant defined by Eq. 6, dimensionless
L	half thickness of electrode, cm
M	the total mass of the electrode, g
Q_o	the initial charge in the electrode, C g^{-1}
Q_1	the charge remaining in the electrode after discharge, C g^{-1}
r	distance from the center of the spherical particle, cm
R	gas constant, 8.314 J, (mol K)$^{-1}$
R_p	polarization resistance, Ω g
t	time, s
T	temperature, K
v	sweep rate, V s^{-1}

Greek

β	symmetry factor, dimensionless
η	overpotential, V
τ	transient time, s

Subscript

b	bulk of the electrolyte
i	interface of the electrolyte/electrode
p	pores of the electrode

REFERENCES

1. H. F. Bittner and C. C. Badcock, *This Journal*, **130**, 193C (1983).
2. J. J. G. Willems, *Philips J. Res.*, **39**, Suppl. 1, 1 (1984).
3. *Hydrides for Energy Storage*, A. F. Andersen and A. J. Maeland, Editors, Proceeding of an International Symposium, International Association for Hydrogen Energy, Pergamon Press, Oxford (1978).
4. *Metal-Hydrides Systems. Fundamentals and Applications*, R. Kircheim, E. Fromm, and E. Wicke, Editors, Proceedings of the First International Symposium combining "Hydrogen in Metals" and "Metal

Hydrides," Stuttgart, Federal Republic of Germany (1988).
5. H. Yayama, K. Kuroki, K. Hirakawa, and A. Tomokiyo, *Jpn. J. Appl. Phys.*, **23,** 1619 (1984).
6. P. H. L. Notten and P. Hokkeling, *This Journal,* **138,** 1877 (1991).
7. M. Ciureanu, D. H. Ryan, J. O. Ström-Olsen, and M. L. Trudeau, *ibid.*, **140,** 579 (1993).
8. H. Yayama, K. Hirakawa, and A. Tomokiyo, *Jpn. J. Appl. Phys.*, **25,** 739 (1986).
9. M. H. J. Van Rijswick, in *Hydrides for Energy Storage,* Proceeding of an International Symposium, A. F. Anderson and A. J. Maeland, Editors, p. 261, International Association for Hydrogen Energy, Pergamon Press, Oxford (1978).
10. T. Sakai, H. Ishikawa, K. Oguro, C. Iwakura, and H. Yoneyama, *This Journal,* **134,** 558 (1987).
11. H. Zuchner, T. Rauf, and R. Hempelmann, *J. Less-Common Met.*, **172-174,** 611 (1991).
12. M. H. Mendelsohn, D. M. Gruen, and A. E. Dwight, *Mater. Res. Bull.*, **13,** 1221 (1978).
13. D. Chandra and F. Lynch, *Rare Earths,* p. 83, The Metallurgical Society, Warrendale, PA (1988).
14. S. W. Lambert, D. Chandra, W. N. Cathey, F. E. Lynch, and R. C. Bowman, Jr., *J. Alloys Compounds,* **187,** 113 (1992).
15. B. V. Ratnakumar, C. Witham, B. Fultz, and G. Halpert, *This Journal,* **141,** L89 (1994).
16. L. G. Austin, *Trans. Faraday Soc.*, **60,** 1319 (1964).
17. L. G. Austin and H. Lerner, *Electrochim. Acta,* **9,** 1469 (1964).
18. P. A. Allen and A. Hickling, *Trans. Faraday Soc.*, **53,** 1626 (1957).
19. A. J. Bard and L. R. Faulkner, *Electrochemical Methods-Fundamentals and Applications,* p. 106, John Wiley & Sons, Inc., New York (1980).
20. G. Zheng, B. N. Popov, and R. E. White, *This Journal,* **142,** 2695 (1995).

A Quartz Crystal Microbalance Probe Developed for Outdoor *In Situ* Atmospheric Corrosivity Monitoring

M. Forslund and C. Leygraf*

Department of Materials Science and Engineering, Division of Corrosion Science, Royal Institute of Technology, S-100 44 Stockholm, Sweden

ABSTRACT

In order to perform *in situ* monitoring of minute corrosion attacks during outdoor field exposures, an atmospheric corrosivity probe has been developed based on the quartz crystal microbalance. A remotely controlled computerized mobile field station was also constructed. The whole setup allows simultaneous *in situ* measurements of mass changes with a resolution of ± 10 ng cm^{-2}, and of climatic parameters. The observed mass changes during introductory exposures of gold and copper in an urban atmosphere are both reversible and irreversible. Aided by *ex situ* x-ray photoelectron spectroscopy analysis, the results can be interpreted in terms of salt deposition, water adsorption, water desorption, and atmospheric corrosion effects.

Introduction

The increased use of electrical or electronic equipment in environments with higher levels of atmospheric pollutants is a major concern for the reliability of such equipment. To assess the problem and make proper countermeasures, the atmospheric corrosivity needs to be known with respect to the metals used in electronics. Consequently, there is a need for highly sensitive methods with the ability to monitor the corrosivity in the actual field environments where the equipment is used.

Evaluation of the corrosivity in a given indoor or outdoor environment is normally performed either by determining the corrosion attack on small plates or coupons of different metals exposed to the atmosphere or by monitoring the most important gaseous pollutants. Analysis of exposed metal coupons provides direct information of the corrosion processes actually in progress. For qualitative analysis, several different analytical techniques are available. Two examples are x-ray photoelectron spectroscopy (XPS) and Auger electron spectroscopy (AES). Evaluation methods commonly used for quantitative determination are measurements of weight gain, weight loss, or cathodic reduction of corrosion products. The major drawback with coupon exposure is that all measurements are performed *ex situ*. Also, the detection limit for weight change in field exposures, around 10^{-6} g cm^{-2}, requires extensive exposure times. Thus, the time resolution for consecutive exposures with coupons is at least months or, sometimes, years.

Pollutant monitoring, on the other hand, is often performed *in situ*, thus, giving information on the variation in pollutant levels on an hourly or daily basis. Drawbacks are the high cost of equipment and sometimes also the lack of knowledge of the possible influence of the measured pollutant on the corrosion process in the actual case. Several different gases are often needed to explain corrosion attacks on a given metal, from which follows that the cost of equipment is increased with each gas.

An attractive alternative would be a method which combines the benefits of the two approaches, generating the direct corrosion information of the coupons and the continuous *in situ* sampling of the gas analysis while being applicable both indoors and outdoors. Several techniques have been elaborated to achieve this combination by measuring corrosivity in terms of changes in resistivity, electrochemical current, or frequency.

Mikhailovskii *et al.*[1] proposed a method for continuously recording the rate of atmospheric corrosion outdoors using the resistance change arising from the atmospheric corrosion of thin metal layers or foils. Two types of sensors with iron surfaces were constructed, having either high resolution or accepting high mass load. The mass resolution of these sensors were $1 \cdot 10^{-2}$ and $2 \cdot 10^{-2}$ g cm^{-2}, respectively.

González *et al.*[2] determined the polarization resistance and Tafel slopes from a modified electrochemical atmospheric corrosion monitor having a three-electrode system. These sensors consist of stacked metal foils insulated from each other by encapsulation in a resin that leaves thin resin layers intercalating the metal foils, exposing only the edges of one side of the foils. Surfaces of iron were exposed outdoors. The sensitivity depends on many parameters, such as corrosion rate, cell geometry, and thickness of the moisture layer, and cannot easily be estimated. Similar electro-

* Electrochemical Society Active Member.